Phase Stability of Nanolaminated Epitaxial $(Cr_{1-x}Fe_x)_2AlC$ MAX Phase Thin Films on MgO(111) and Al_2O_3(0001) for Use as Conductive Coatings

Hanna Pazniak[*,§], *Marc Stevens*[§], *Martin Dahlqvist*[#], *Benjamin Zingsem*[§,⁄⁄], *Lidia Kibkalo*[⁄⁄],

Merve Felek[§], *Sergey Varnakov*[⊥], *Michael Farle*[§,⊥], *Johanna Rosen*[#], *Ulf Wiedwald*[*,§]

[§]Faculty of Physics and Center for Nanointegration (CENIDE), University of Duisburg-Essen, 47057 Duisburg, Germany

[#]Materials Design, Department of Physics, Chemistry, and Biology (IFM), Linköping University, SE-581 83 Linköping, Sweden

[⁄⁄]Ernst Ruska-Centre for Microscopy and Spectroscopy with Electrons (ER-C), Forschungszentrum Jülich, 52425 Jülich, Germany

[⊥]Kirensky Institute of Physics, Federal Research Center KSC SB RAS, Krasnoyarsk, 660036, Russian Federation

KEYWORDS: MAX phase, thin film, DFT calculations, Pulsed Laser Deposition, TEM/EDX, electrical resistivity

ABSTRACT: In this study, we model the chemical stability in the $(Cr_{1-x}Fe_x)_2AlC$ MAX phase system using density functional theory predicting its phase stability for $0 < x < 0.2$. Following the calculations, we have successfully synthesized nanolaminated $(Cr_{1-x}Fe_x)_2AlC$ MAX phase thin films with a target Fe content of $x = 0.1$ and $x = 0.2$ by Pulsed Laser Deposition using elemental targets on MgO(111) and Al_2O_3(0001) substrates at 600 °C. Structural investigations by X-ray diffraction and transmission electron microscopy reveal MAX phase epitaxial films on both substrates with a coexisting $(Fe,Cr)_5Al_8$ intermetallic secondary phase. Experiments suggest an actual maximum Fe solubility of 3.4 at%, corresponding to $(Cr_{0.932}Fe_{0.068})_2AlC$, which is the highest Fe doping level achieved so far in volume materials and thin films. Residual Fe is continuously distributed in the $(Fe,Cr)_5Al_8$ intermetallic secondary phase. The incorporation of Fe results in the slight reduction of the c lattice parameter while the a lattice parameter remains unchanged. The nanolaminated $(Cr_{0.932}Fe_{0.068})_2AlC$ thin films show metallic behavior and can serve as promising candidates for highly conductive coatings.

INTRODUCTION

MAX phases are a rapidly expanding family of thermodynamically stable ternary carbides and nitrides with atomically layered structure and chemical formula $M_{n+1}AX_n$, where M is an early transition metal, A is an A-group element (e.g. Al, Si, Ga, Ge, etc.), and X is carbon or nitrogen [1-2]. MAX phase compounds are known for their notable potential in high temperature applications since they exhibit stability, thermal shock resistance, good mechanical properties, and excellent thermal and electrical conductivity under harsh conditions [3]. To date, about 155 MAX phase compositions and their solid solutions have been successfully synthesized [2].

Introducing additional elements into MAX phase structures thereby expands their chemistry and allows to master mechanical [4-5], optical [6] or magnetic properties [7-9]. Doping can promote

incorporation of previously excluded elements for MAX phases (e.g. lanthanides) leading to the formation of nanolaminated chemically ordered structures (out-of-plane and in-plane) with new structural and magnetic characteristics [10-12]. On the other hand, doping with late 3d-elements like Mn or Fe results in the partial substitution of parental M-sites elements forming a solid solution. This approach has been successfully used to fine tune metallic and/or ceramic characteristics or to introduce intriguing features such as magnetic order. The latter will further expand the numerous applications of MAX phases towards spintronics, magneto-transport [13], magneto-calorics or as magneto-strictive components [14].

To date, Mn_2GaC is the only compound incorporating Mn as a sole M-element demonstrating magnetic order [15,16]. In further search for magnetic MAX phases, several attempts were made to synthesize solid solutions in volume materials or as thin films focusing on the introducing of Mn or Fe on M [17-18] or A [19-20] sublattices sites of MAX phases. Until now, the most promising results are shown for Ge and Ga based MAX phases demonstrating the existence of long-range magnetic order in nano-layered $(Cr_{0.96}Mn_{0.04})_2GeC$ and in $(Cr_{0.93}Mn_{0.07})_2GaC$ powder compounds [21]. Moreover, introducing Fe (up to x = 0.125) and Mn (up to x = 0.25), as well as Ti (up to x = 0.25) and Mo (up to x = 0.375) in the $(Cr_{1-x}M_x)_2GeC$ MAX phase induces long range magnetic order in the initially paramagnetic Cr_2GeC MAX phase sample [22]. Addition of Mn to bulk polycrystalline $(Cr_{1-x}Mn_x)_2GaC$ MAX phase ($0 \leq x \leq 0.5$) allows to tailor magnetic characteristics from paramagnetic (x=0) to ferrimagnetic (x=0.5) [23]. For Al-based MAX phases, doping of Fe [17] and Mn [24] has an upper limit of 2-3 at.% incorporated into the structure of V_2AlC and Cr_2AlC parent compounds. Despite these successful doping experiments, a ferro- or ferrimagnetic ground state of the MAX phases has not been found. Further increase of Mn and Fe content beyond the 2 at.%

limit leads to the formation of additional side phases being responsible for a ferromagnetic behavior of the corresponding bulk materials.

In this respect the synthesis of MAX phase thin films is favorable as compared to their bulk counterparts due to improved phase purity, high crystalline quality, and controlled orientation through epitaxial growth. This facilitates the in-depth study of doping in the hexagonal nanolaminated MAX phase structure and the related magnetic properties. For epitaxial $(Cr_{0.5}Mn_{0.5})_2GaC$ MAX phase thin films, a temperature dependent ferromagnetic component with negligible magnetocrystalline anisotropy has been reported [25]. Moreover, experiments have shown that the Mn solubility in Cr_2AlC is lower in the bulk with a maximum of 3 at.% ($(Cr_{0.94}Mn_{0.06})_2AlC$ [26] as compared to corresponding thin films reporting a maximum of 10 at.% ($(Cr_{0.8}Mn_{0.2})_2AlC$) using arc deposition [18].

The aforementioned factors drive the research towards the development of adopted and improved thin film deposition techniques for the growth of epitaxial MAX phases. Furthermore, the solubility of the late transition metals in MAX phases might be enhanced by physical vapor deposition if the film growth is performed far from thermodynamic equilibrium.

Recently we successfully demonstrated that the high energy (up to 100 eV) of ablated species obtained during Pulsed Laser Deposition (PLD) results in good mixture of deposited elements allowing to grow epitaxial Cr_2AlC thin films with precise chemical composition [27].

Future application concepts for magnetic MAX phases, as discussed above, demand the understanding of intrinsic properties and their anisotropy. Based on the experience from growing phase pure and epitaxial Cr_2AlC thin films by PLD, we use this as parent compound to study the Fe doping of $(Cr_{1-x}Fe_x)_2AlC$ thin films (with the target amount in the MAX phase structure of x = 0.1 and 0.2) on MgO(111) and Al_2O_3(0001) substrates. The structure and morphology of the Fe-

doped Cr_2AlC MAX phase is investigated on the micro- and nanoscale level by X-ray diffractometry (XRD), XRD pole figures, scanning electron microscopy (SEM), atomic force microscopy and high-resolution transmission electron microscopy (HRTEM). Electrical measurements reveal metallic conductivity of the synthesized film typical for MAX phases suggesting their potential in high temperature applications as conductive coatings. In this study we prove that PLD is a well-suited technique to incorporate Fe in the nanolaminate structure of Cr_2AlC MAX phases and thereby fine tune their properties.

METHODS

Computation methods. First-principles calculations were performed by means of density functional theory (DFT) and the projector augmented wave method [28-29] as implemented in the Vienna ab-initio simulation package (VASP) version 5.4.1 [30-32]. The spin-polarized generalized gradient approximation (GGA) has been used as parameterized by Perdew–Burke–Ernzerhof (PBE) to incorporate the electron exchange and correlation effects [33]. We consider selected spin configurations based on results for Cr_2AlC [34-35], namely ferromagnetic (FM) and several antiferromagnetic (AFM) configurations; multilayered AFM ordering of α consecutive *M* layers (where α = 2) with the same spin direction before changing sign upon crossing an Al layer ($AFM[0001]_2^A$) and antiparallel spins within one *M* layer (in-AFM1). The plane wave energy cutoff was set to 400 eV for k-point grids with a spacing of 0.05 $Å^{-1}$ according to the Monkhorst-Pack method [36]. The total energy is minimized through relaxation of the unit-cell shape and volume, and internal atomic positions until reaching an energy convergence of 10^{-6} eV/atom. To model chemical disorder or solid solution of Cr and Fe on the *M* sublattice for $(Cr_{1-x}Fe_x)_2AlC$, we used the special quasi-random structure (SQS) method [37] with supercell sizes consisting of 2x2x2,

4x2x1, 4x3x1 and 4x4x1 unit cells, i.e. 64 to 128 atoms per supercell. Convergency tests show that the supercells used give a qualitatively accurate representation and a quantitative convergency in terms of calculated formation enthalpies and lattice parameters. The thermodynamic stability of quaternary MAX phases is investigated at 0 K with respect to decomposition into any combination of competing phases. The most competing set of such, denoted equilibrium simplex, is identified using a linear optimization procedure [38-39] which have been proven successful to confirm already experimentally known MAX phases as well as predicting the existence of new ones [15, 18, 39-42]. The stability of the quaternary MAX phase is quantified in terms of formation enthalpy ΔH_{cp} by comparing its energy to the energy of the equilibrium simplex according to:

$$\Delta H_{cp}^{disorder} = E(MAX) - E(\text{equilibrium simplex})\,. \quad (1)$$

A phase is concluded stable when $\Delta H_{\mathrm{cp}} < 0$. However, when $T \neq 0$ K, the contribution from configurational entropy due to disorder of Cr and Fe on the *M* sublattice will decrease the Gibbs free energy $\Delta G_{\mathrm{cp}}^{\mathrm{disorder}}$ as approximated by

$$\Delta G_{cp}^{disorder}[T] = \Delta H_{cp}^{disorder} - T\Delta S, \quad (2)$$

where the entropic contribution ΔS, assuming an ideal solution of Cr and Fe on *M*-sites, is given by

$$\Delta S = -2\mathrm{k_B}[x\ln(x) + (1-x)\ln(1-x)], \quad (3)$$

where k_B is the Boltzmann constant and x is the concentration of Fe on the M-sublattice.

Synthesis. In the following study doping amounts denoted as x refer to the target Fe content in the MAX phase structure, corresponding to the formula $(Cr_{0.9}Fe_{0.1})_2AlC$ (x=0.1) and $(Cr_{0.8}Fe_{0.2})_2AlC$ (x=0.2). The growth of aforementioned MAX phase thin films was carried out in ultra-high vacuum (base pressure < $1 \cdot 10^{-8}$ mbar) by PLD [43]. An KrF Excimer Laser (wavelength 248 nm) hits pure elemental targets of chromium (Cr, 99,95%), aluminium (Al, 99,99%), iron (Fe, 99,995%) and pyrolytic graphite (C, 99,999%), purchased from Kurt J. Lesker (USA), at an energy density of 13 J cm^{-2}. The MAX phase thin films were grown by sequential layer by layer deposition with a simultaneous decrease of Cr while introducing Fe, corresponding to a ratio of 2-2x : 2x : 5 : 1 ($0.1 \leq x \leq 0.2$) for Cr, Fe Al, and C, respectively, on MgO(111) and Al_2O_3(0001) substrates at 600°C as an optimized growth temperature for the parent Cr_2AlC compound [27]. The amount of Al was set five times higher as compared to the stoichiometric value due to (i) the tendency of Al droplet formation; (ii) the high substrate temperature resulting in thermal desorption of Al and (iii) re-sputtering effects of lighter elements during deposition [27]. The deposition rate was monitored using a quartz crystal monitor.

Experimental Techniques. Structural characterization of the thin films was performed by XRD in Bragg-Brentano geometry using a Panalytical X'Pert MPD PW3040 and an Empyrean MRD device equipped with a Cu-K_α sources (λ = 1.5406 Å) in Θ-2Θ geometry with 0.01° steps, ranging from $10° \leq 2\Theta \leq 90°$. The in-plane epitaxial relation between substrate and MAX phase was determined by pole figures measurements.

The surface morphology of the epitaxial films was studied using SEM and atomic force microscopy, employing Zeiss LEO 1530 and Park Systems XE70 microscopes, respectively. The average chemical composition of the grown thin films was determined using energy dispersive X-ray spectroscopy (EDX) equipped with an Oxford Instruments XMAX 80 mm^2 detector in the SEM. Surface roughness measurements by atomic force microscopy were performed in non-contact (tapping) mode using an ACTA10M type cantilever with a tip radius of 6 nm. The roughness was determined for individual islands in a scan area of 1 µm x 1 µm using the WSxM 5.0 Develop 9.1 software.

For the TEM studies, a cross-section TEM lamella of a $(Cr_{0.9}Fe_{0.1})_2AlC$ thin film on MgO(111) was prepared using Ga focused ion beam (FIB) cutting. The preparation process (lift-out method) consisted of depositing a carbon protective layer, cutting the slice perpendicular to the surface, lifting out of the slice with the help of a micromanipulator, attaching the specimen onto a Cu TEM supporting grid, and final polishing of the lamella to the desired dimensions and thicknesses. The accelerating voltage (5 – 30 keV) and beam current (2.8 nA – 48 pA) were optimized to prepare ultra-thin TEM-specimens. Bright-field (BF) HRTEM and scanning TEM (STEM) images were acquired with a Jeol 2200FS transmission electron microscope at an acceleration voltage of 200 kV using a 2k x 2k GATAN UltraScan®1000XP CCD camera. The local chemical composition of the $(Cr_{0.9}Fe_{0.1})_2AlC$ thin film was determined using EDX in STEM mode with an Oxford windowless 80 mm^2 SDD X-MaxN 80 TLE detector with 0.21 sr solid angle.

Resistivity measurements were performed in four-point geometry using a custom-built sample holder under He atmosphere at p_{He} = 30 mbar in a Physical Property Measurement System (PPMS) DynaCool system in the range of 2-300 K. The spring-tip contacts were pressed onto the film surface and fixed at a distance between the contacts of 2 mm. The magnetic properties of the films

were studied by vibrating sample magnetometry in the PPMS system. 2.5x2.5 mm^2 film on 0.5 mm thick $Al_2O_3(0001)$ was glued on a glass sticker holder and magnetic hysteresis loops at various temperatures were recorded.

RESULTS AND DISCUSSION

Theory and computation. Phase stability calculations have been conducted for the $(Cr_{1-x}Fe_x)_2AlC$ MAX phase with $0 < x < 1$. For each composition we consider three different spin configurations: FM, $AFM[0001]_2^A$ and in-AFM1. Figure 1 shows the calculated formation enthalpy ΔH, at T = 0 K, using Eq. 1 where the identified the equilibrium simplex is listed in Table S1. It is found that ΔH increases with increasing Fe content and at x = 1, Fe_2AlC is found to be far from stable with ΔH = +78 meV/atom. This is consistent with previous reports [44-45]. However, since the focus is on a solid solution of Cr and Fe on the M-sites and that we grow MAX phase epitaxial films at elevated temperature, we discuss stability results related to the Gibbs free energy of formation, ΔG. It has previously been demonstrated that entropy has a stabilizing impact on the formation of solid solutions in quaternary MAX phases upon alloying [41-42, 44]. An increased temperature will thus decrease ΔG for the solid solution $(Cr_{1-x}Fe_x)_2AlC$ due to configurational entropy. Here ΔG is estimated for T from 500 to 2000 K. A temperature of 1500 K and higher is required to thermodynamically stabilize $(Cr_{1-x}Fe_x)_2AlC$, i.e. to get $\Delta G < 0$. At 1500 K, ΔG is around zero for $x < 0.2$ indicating that the solid solution $(Cr_{1-x}Fe_x)_2AlC$ is stabilized by temperature. Further increase of T to 2000 K results in stable solid-solution $(Cr_{1-x}Fe_x)_2AlC$, $\Delta G < 0$, for $x < 0.45$. In short, the results shown in Figure 1 demonstrate that small amounts of Fe, $x < 0.2$ for T = 1500 K, could be incorporated in Cr_2AlC.

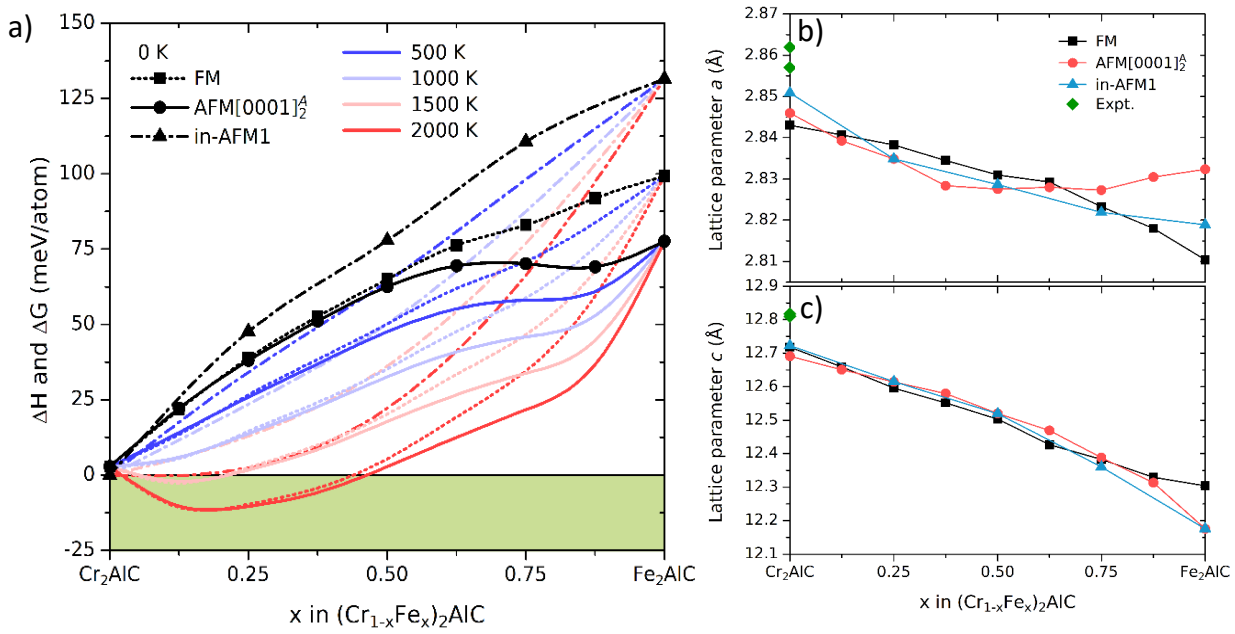

Figure 1. (a) Calculated formation enthalpy, ΔH, at 0 K and Gibbs free energy of formation, ΔG, estimated at 500 to 2000 K for $(Cr_{1-x}Fe_x)_2AlC$ for selected spin configurations. Calculated lattice parameters (b) a and (c) c for $(Cr_{1-x}Fe_x)_2AlC$ for selected spin configurations. Experimental values are shown by green diamonds [46-47].

Figure 1, panels b and c show the calculated lattice parameters *a* and *c* for $(Cr_{1-x}Fe_x)_2AlC$ for the considered spin configurations. In addition, experimentally reported values for Cr_2AlC are included as reference [46-47]. In the region of interest, $x < 0.45$, both lattice parameter *a* and *c* decrease with increasing Fe content independent of the spin configuration.

Our DFT findings give the main motivation for the following experimental investigation of the solubility of the Fe in Cr_2AlC MAX phase thin films. We have chosen to introduce x = 0.1 and 0.2 of Fe in the $(Cr_{1-x}Fe_x)_2AlC$ MAX phase in the previously developed protocol for epitaxial growth of Cr_2AlC on MgO(111) and Al_2O_3(0001).

Growth and characterization of $(Cr_{1-x}Fe_x)_2AlC$ thin films. Metallic thin films with nominal thickness of 40 nm are simultaneously grown on MgO(111) and Al_2O_3(0001) substrates at a deposition temperature of 600 ˚C using Cr, Fe, Al, and C elemental targets as described in more detail in the Methods section and schematically depicted in Figure 2.

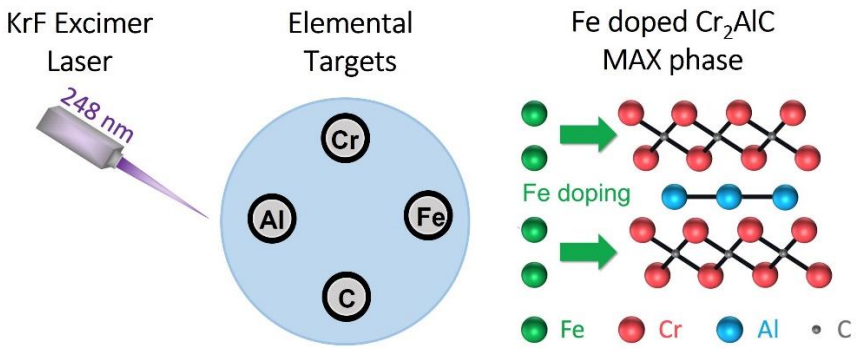

Figure 2. Schematic illustration of the thin film growth of the Fe doped Cr_2AlC MAX phase. The process includes the ablation from pure elemental targets using a KrF excimer laser resulting in the incorporation of Fe atoms in the layered structure of the parent Cr_2AlC MAX phase.

The thickness of 40 nm is chosen above the percolation limit for the parent Cr_2AlC MAX phase thin films suggesting the formation of continuous metallic conductive films [27]. The surface morphology is studied by SEM and atomic force microscopy. Representative SEM images of the $(Cr_{0.9}Fe_{0.1})_2AlC$ and $(Cr_{0.8}Fe_{0.2})_2AlC$ films grown on MgO(111) and Al_2O_3(0001) are shown in Figure 3 a, b and c, d respectively. Corresponding height profile atomic force microscope images are depicted accordingly in the Figure 3 e-h.

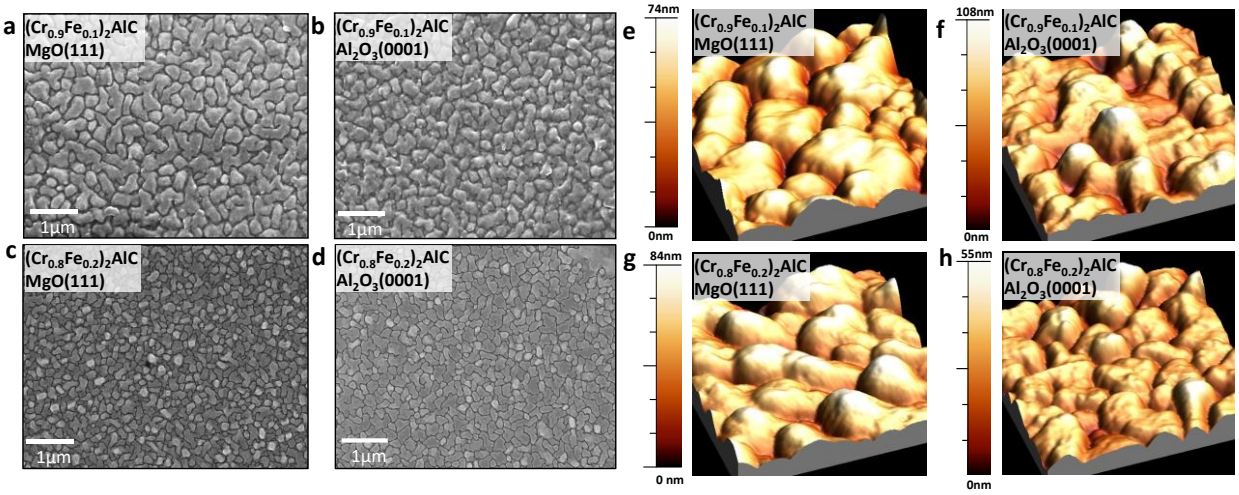

Figure 3. Top view SEM images of $(Cr_{0.9}Fe_{0.1})_2AlC$ (a, b) and $(Cr_{0.8}Fe_{0.2})_2AlC$ (c, d) thin films on MgO(111) and Al_2O_3(0001) substrates and corresponding height profile atomic force microscopy images (e-h).

The films grown on MgO(111) and Al_2O_3(0001) substrates exhibit a continuous coverage with a well-resolved film morphology, consisting of differently sized coalescent grains. A higher targeted Fe concentration of $x = 0.2$ results in smaller grains as compared to $x = 0.1$. A columnar growth mode is evident by the atomic force microscopy images, revealing an almost substrate and doping independent roughness of the MAX phase grains ranging from (0.6 ± 0.1) nm to (1.3 ± 0.2) nm for films on MgO(111) and (1.0 ± 0.1) nm to (1.4 ± 0.2) nm for films grown on Al_2O_3(0001), respectively (Table 1). As determined by SEM-EDX, the elemental distribution within $(Cr_{0.9}Fe_{0.1})_2AlC$ and the $(Cr_{0.8}Fe_{0.2})_2AlC$ film grains is homogeneous revealing the targeted Fe/(Cr+Fe) ratio of 0.1 and 0.2, respectively. See Supporting Information, Figures S1 and S2 for details. Elemental mapping shows no clustering of Fe within the films nor at the grain boundaries on the µm scale. However, the $(Cr_{0.8}Fe_{0.2})_2AlC$ film exhibits a visible phase inhomogeneity due to the presence of melt-like regions, possibly attributed to the intermetallic solid solution (see Supporting Information, Figure S3).

Figure 4 displays the XRD patterns of a 36 nm pure Cr_2AlC film and 40 nm thick $(Cr_{1-x}Fe_x)_2AlC$ films with x = 0.1 and x = 0.2 grown on MgO(111) and Al_2O_3(0001). For the reference Cr_2AlC parent MAX phase (blue curve) and $(Cr_{0.9}Fe_{0.1})_2AlC$ films (green and violet curves), PLD results in the formation of phase pure highly textured films since only (000*l*) MAX phase peaks are visible with no traces of other crystalline phases. As the Fe concentration increases up to x = 0.2 (red and black curves), additional peaks appear, which we identified as Fe_5Al_8 (*ICSD CollCode 169545*) or its solid solution with Cr_5Al_8 *(ICSD CollCode184444)*. These phases may also have peaks overlapping with the MAX phase [26], as discussed further below. We note that the formation of the intermetallic compound (Fe_5Al_8) is theoretically predicted being a competitive phase in the Cr-Fe-Al-C system (see Supporting Information, Table S1).

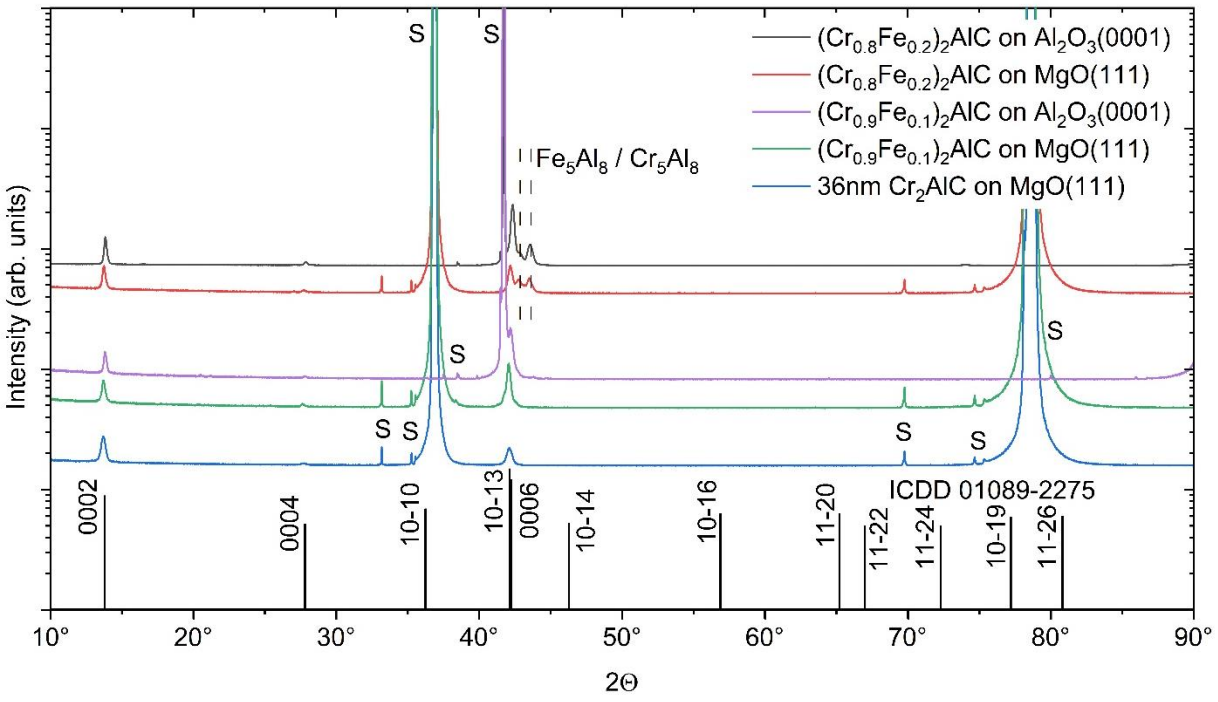

Figure 4. XRD θ–2θ scans for 40 nm $(Cr_{0.9}Fe_{0.1})_2AlC$ (green and violet curves) and $(Cr_{0.8}Fe_{0.2})_2AlC$ (red and grey curves) films deposited on Al_2O_3(0001) and MgO(111) substrates at 600°C. Substrate peaks are marked with a 'S' symbol. XRD of the 36 nm thick Cr_2AlC film

(blue curve) is placed for comparison. Sticks and Miller indices reflect the angular position of Cr_2AlC powder (ICDD 01089-2275).

Further, we investigate the expected epitaxial relations of $(Cr_{1-x}Fe_x)_2AlC$ thin films by pole figure measurements (Figure 5). The 10-13 XRD pole figure of $(Cr_{0.9}Fe_{0.1})_2AlC$ on MgO(111) recorded at ψ angle between 50 and 60° (Figure 5a, outer ring) displays the expected three strong intense peaks at ψ angle ~ 55° originating from MgO(111) and revealing three-fold symmetry. Less intense six peaks partially overlapping the MgO peaks are attributed to the MAX phase [27]. Low intensity peaks (light blue circles) located in the vicinity to the main MAX phase peaks are depicted and possibly appear due to the presence of small number of grains deviating from [11-20] in-plane orientation [48]. Interestingly, the $(Cr_{1-x}Fe_x)_2AlC$ MAX phase and Cr_5Al_8 based solid solutions (bcc structure) can coexist in the thin film. These, however, cannot be distinguished by conventional XRD and pole figures, since interplanar spacing of Cr_5Al_8 based solid solution matches exactly half a unit cell of Cr_2AlC [26]. Thus, we additionally perform pole figure measurements between ψ = 32° and 35° (Figure 5a). Peaks at this ψ angle position exist only for intermetallic Cr_5Al_8 based bcc structures and not for the MAX phases structure [26]. The results presented in Figure 5a (inner ring) do not show any peaks apart from the background, revealing the phase purity of the synthesized thin films and in-plane epitaxial relation $(Cr_{0.9}Fe_{0.1})_2AlC$[11-20] || MgO [10-1]. The pole figure of $(Cr_{0.9}Fe_{0.1})_2AlC$ grown on Al_2O_3(0001) in Figure 5b shows the presence of the central (0006) MAX phase peak and 6 sharp intense reflections originating from the {11-23} planes in sapphire overlapping with (10-13) MAX peaks, as discussed in more detail in Ref. [27]. Like the film on MgO(111), no additional diffraction peaks are detected at ψ-angles 32°-35°, suggesting the formation of phase pure $(Cr_{0.9}Fe_{0.1})_2AlC$ on Al_2O_3(0001).

For increased Fe content in $(Cr_{0.8}Fe_{0.2})_2AlC$ films, the pole figures change for both substrates, MgO(111) and Al_2O_3(0001) (Figures 5c,d). In Figure 5c for the $(Cr_{0.8}Fe_{0.2})_2AlC$ on MgO(111), we clearly detect broad peaks grouped in doublets around positions of $(Cr_{0.9}Fe_{0.1})_2AlC$ film (cf. Figure 5a). Such pattern suggests two in-plane orientations of MAX phase grains with respect to MgO(111). Since the presence of secondary phases significantly influences the film epitaxy, simultaneous growth of two phases may cause higher stress in the MAX phase grains resulting peak broadening.

The 10-13 pole figure of $(Cr_{0.8}Fe_{0.2})_2AlC$ on Al_2O_3(0001) in Figure 5d shows 6 high-intense peaks (dark red rectangles) originating from the {11-23} planes in the sapphire substrate [27]. Apart from this, two coupled pairs of less intense circled peaks (red and light blue circles) revealing six-fold symmetry are detected and can be attributed to the epitaxially grown MAX phase and the $(Cr,Fe)_5Al_8$ intermetallic compounds. We note that there is a 30° in-plane rotation of film domains with respect to the Al_2O_3(0001) substrate as compared to the film with lower Fe content. In-plane rotation leads to the stress reduction confirmed by the presence of sharp circled peaks. The existence of the $(Cr,Fe)_5Al_8$ phase is evident by the well-defined six peak pairs at the ψ = 32°-35° (Figure 5d, inner ring) [26].

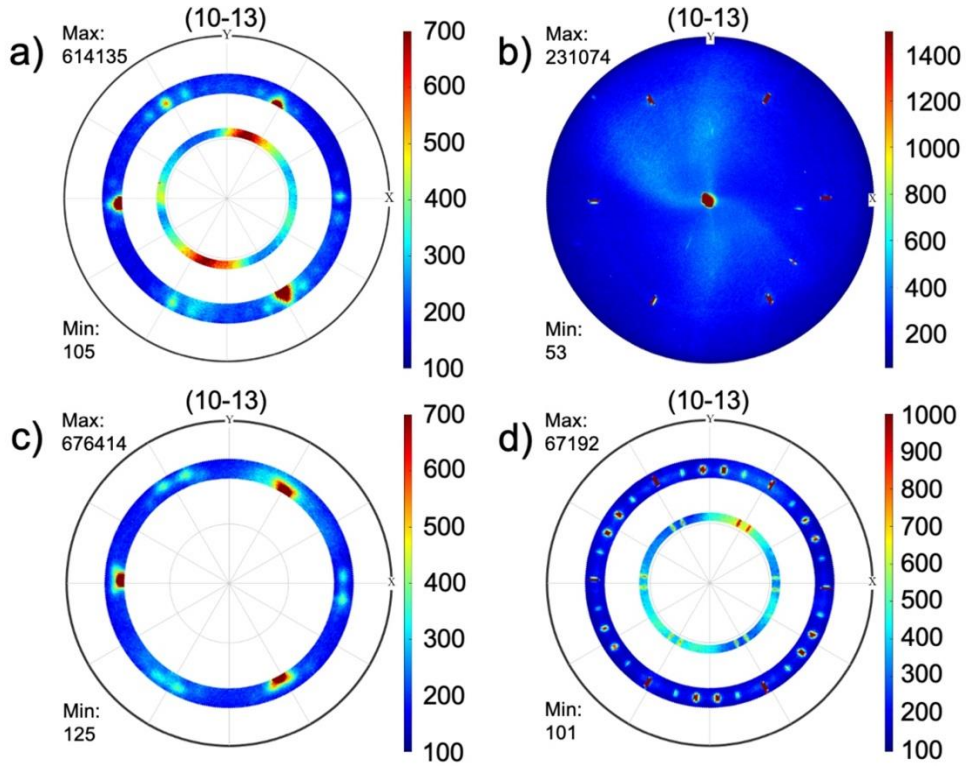

Figure 5. The 10-13 XRD pole figure of $(Cr_{0.9}Fe_{0.1})_2AlC$ (a) on MgO(111) recorded at ψ angle 50-60° and 30-35° and (b) on Al_2O_3(0001) at ψ angle 0-90°, (c) the 10-13 XRD pole figure of $(Cr_{0.8}Fe_{0.2})_2AlC$ film on MgO(111) recorded at ψ angles 50°-60° and (d) on Al_2O_3(0001) recorded at ψ angle between 50°-60° and 30°-35°.

Based on the XRD data and pole figures we calculated the lattice parameters of the MAX phase films and the XRD coherence length (Table 1). Incorporation of Fe in the Cr_2AlC MAX phase results in a slight reduction of the *c* lattice parameter (Figure 1c) and has a similar, but less pronounced effect on the *a* lattice parameter. This is in line with the computational findings predicting the gradual decrease in the *a* and *c* lattice parameters with increasing amount of Fe (Figure 1b,c). The calculated XRD coherence length of the film is reduced compared to the nominal thicknesses, however, still suggests single crystalline growth along the *c* axis.

Table 1. Lattice parameters and XRD coherence length of $(Cr_{0.9}Fe_{0.1})_2AlC$ and $(Cr_{0.8}Fe_{0.2})_2AlC$ films grown on MgO(111) and Al_2O_3(0001) substrates, and the root mean square (RMS) roughness of the grains.

Sample	c-Parameter [nm]	a-Parameter [nm]	Coherence length [nm]	RMS roughness [nm]
$(Cr_{0.9}Fe_{0.1})_2AlC$ on MgO(111)	1.282± 0.004	0.286± 0.010	29± 2	1.3±0.2
$(Cr_{0.9}Fe_{0.1})_2AlC$ on Al_2O_3(0001)	1.278± 0.004	0.285± 0.010	35± 3	1.4±0.2
$(Cr_{0.8}Fe_{0.2})_2AlC$ on MgO(111)	1.279± 0.004	0.285± 0.010	32± 3	0.6±0.1
$(Cr_{0.8}Fe_{0.2})_2AlC$ on Al_2O_3(0001)	1.277± 0.004	0.285± 0.010	37± 3	1.0±0.1

To elucidate the detailed structure of the $(Cr_{0.9}Fe_{0.1})_2AlC$ MAX phase, the film is further studied by HRTEM. In the following, we focus on $(Cr_{0.9}Fe_{0.1})_2AlC$ film due to its XRD phase purity. The structural and compositional results are shown in Figure 6. A typical cross-section HRTEM bright-field image of the $(Cr_{0.9}Fe_{0.1})_2AlC$ thin film on MgO(111) is displayed in Figure 6a. The synthesized film consists of distinct grains as also seen in the SEM top-view images in Figure 3. The columnar growth along the *c* axis is clearly shown with grain heights roughly matching the nominal film thickness and lateral dimension of 25-50 nm. The STEM images in Figures 6b,c indicate the typical MAX phases layered structure exhibiting alternating dark contrast layers (Al atoms) and twin-layered rows of bright contrast (Cr atoms), while the C atoms interleaving the Cr

rows are invisible due to the lower Z-contrast. By recording the EDS line profile along the yellow line in Figure 6c, we distinguish the MAX phase layered structure by the element distributions of Cr, Al, and Fe. Cr and Al layers show up by the alternating EDS intensities along the *c* axis. As expected, the low Fe EDS spectral intensities predominantly appear together with Cr, suggesting the incorporation of Fe in the M layers of the Cr_2AlC MAX phase structure. Interestingly, the Fe concentration increases close to the substrate. The unit cell *c* axis parameter of 1.27 nm agrees with XRD results. Within the layered MAX phase structure, we identify domains with different stacking (Figure 6d, white circle) featuring deviation from the typical zigzag atomic pattern of M-layers in the cross section along the [11-20] zone axis. Such structural feature was earlier observed for $(Cr,Mn)_2AlC$ thin films and explained by the coexistence of $(Cr_{1-x}Mn_x)_5Al_8$ solid solution within the MAX phase domains [26].

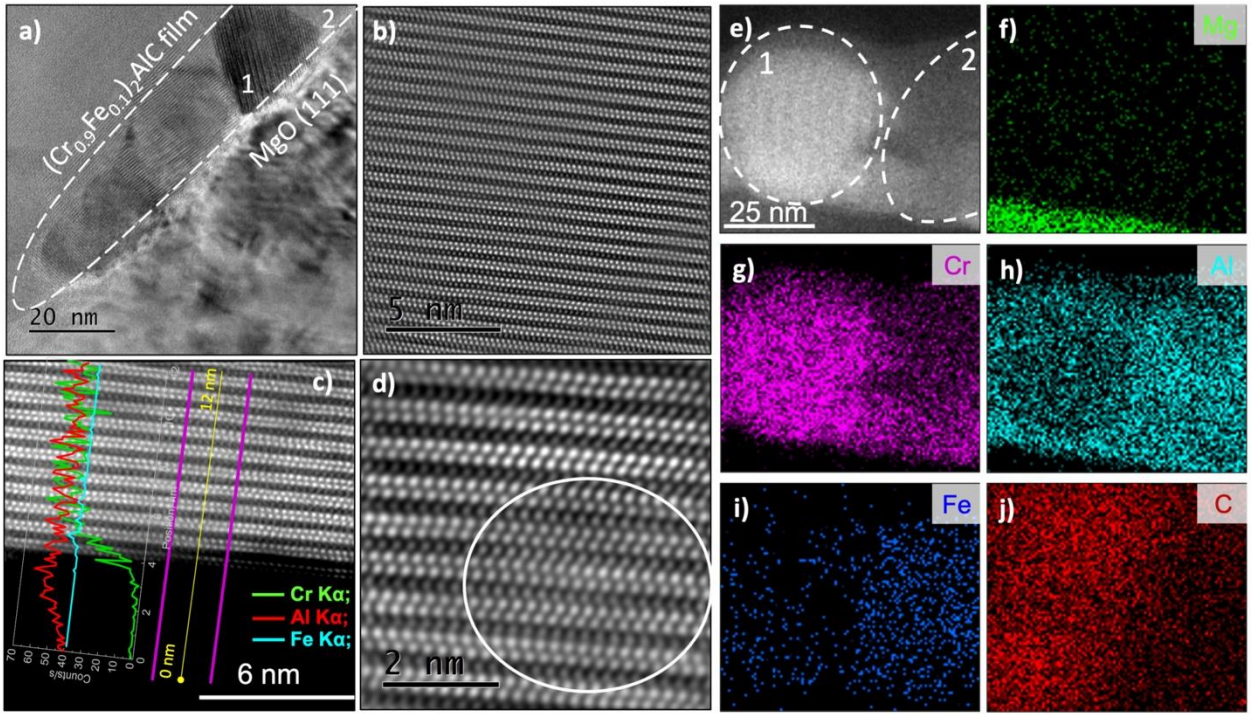

Figure 6. a) High-resolution bright field HRTEM image of $(Cr_{0.9}Fe_{0.1})_{2AlC}$ on MgO(111). b), c), d), e) STEM images of $(Cr_{0.9}Fe_{0.1})_2AlC$ on MgO(111) along the [11-20] zone axis. Panel c) additionally shows an EDS line scan along the c axis. The panels on the right show elemental mappings for Mg (f), Cr (g), Al (h), Fe (i) and C (j).

Elemental mapping of two film grains (Figure 6e) is shown in Figures 6f to 6j and the ratio of the main elements is presented in Table S2. The interface between the substrate (Mg, green) and film is clearly depicted. The elemental distribution on the nanoscale is found to be inhomogeneous in contrary to the microscale analysis performed by SEM-EDS discussed above. The two grains have different compositions, one rich in Cr and C (Region 1, left), which we attribute to the MAX phase and an Fe-rich region with almost no C content and reduced amount of Cr (Region 2, right). Al is rather homogenously distributed in both regions. To attribute the regions to a certain phase we quantify the (Cr+Fe) / Al atomic ratio and the corresponding Fe amounts. The (Cr+Fe)/Al atomic ratio in Region 1 is close to the characteristic MAX phase 2:1 ratio, while in Region 2 it is 1.10-1.34, which is attributed to the solid solution of $(Cr,Fe)_5Al_8$ (Table S2). The solubility of Fe is higher in the $(Cr,Fe)_5Al_8$ solid solution as in the MAX phase with a maximum detected amount of 6.0 at.%. The maximum amount of Fe found in the studied MAX phase structure (in the sample with the target Fe content of x=0.1) is 3.4 at.% ($(Cr_{0.932}Fe_{0.068})_2AlC$), which is the highest value reported to date for both, thin films and bulk samples. Overall, the Fe doping leads to the same behavior as Mn in the Cr_2AlC parent MAX phase which has been investigated by Mockute et al. [26]. $(Cr,Mn)_2AlC$ MAX phase thin films prepared by arc deposition and magnetron sputtering have shown the competitive epitaxial growth of $(Cr_{1-x}Mn_x)_5Al_8$ solid solution and the $(Cr,Mn)_2AlC$ MAX phase.

Such two-phase growth mode should also show up in the magnetic properties of the epitaxial thin films [18]. We measure the magnetic response of the 40 nm $(Cr_{0.9}Fe_{0.1})_2AlC$ MAX phase film on $Al_2O_3(0001)$ and of a similarly treated substrate as a reference by vibrating sample magnetometry (see Supporting Information). Figure S4 (a-c) presents the signals of the solid substrate while (d-f) present the data of the 40 nm film on an identically sized $Al_2O_3(0001)$ substrate. For the bare substrate we obtain e.g. a saturation magnetic moment $\mu = 5 \cdot 10^{-6}$ emu at 300 K, respectively. The magnetic response of the 40 nm $(Cr_{0.9}Fe_{0.1})_2AlC$ on $Al_2O_3(0001)$ is displayed in Figure S4 (d). The room temperature data appears at high quality and after subtraction of the diamagnetic slope a S-shaped hysteresis is obtained as shown in Figure S4 (e). However, the overall sample magnetic moment is only $1 \cdot 10^{-5}$ emu and thus only a factor of 2 above the bare substrate and holder signal in Figure S4 (b). Ascribing this add-on signal to the film, the saturation magnetization of $(Cr_{0.9}Fe_{0.1})_2AlC$ is about 20 emu cm^{-3}. This value is 15 times lower as compared with epitaxial $(Cr_{0.8}Mn_{0.2})_2AlC$ MAX phase thin film ($3.3 \cdot 10^5$ A/m) [18]. The magnification around zero field in Figure S4 (f) shows a slightly open hysteresis loops which is temperature independent which likely originates from the sample holder or the substrate. Based on the small difference between the film on $Al_2O_3(0001)$ and the bare substrate and the unclear contribution of the sample holder we do not dare extracting other magnetic parameters here. Instead, we characterize the electronic transport properties of $(Cr_{0.9}Fe_{0.1})_2AlC$ and $(Cr_{0.8}Fe_{0.2})_2AlC$ films, which have not shown any field-dependent features, and set them in comparison to the parent Cr_2AlC film on MgO(111).

Figure 7 depicts the temperature dependent electrical resistivity for $(Cr_{0.9}Fe_{0.1})_2AlC$ (blue curves) and $(Cr_{0.8}Fe_{0.2})_2AlC$ (red curves) on MgO(111) and $Al_2O_3(0001)$ substrates, as well as for parent Cr_2AlC on MgO(111) as a reference (green curve). All films show metallic behavior with

a decreasing resistivity with temperature from 300 K to 3 K. For the films on Al_2O_3(0001) substrates a low residual resistance ratio (RRR) is found at 1.31 for $(Cr_{0.9}Fe_{0.1})_2AlC$ and 1.25 for $(Cr_{0.8}Fe_{0.2})_2AlC$, which was ascribed before to surface scattering.

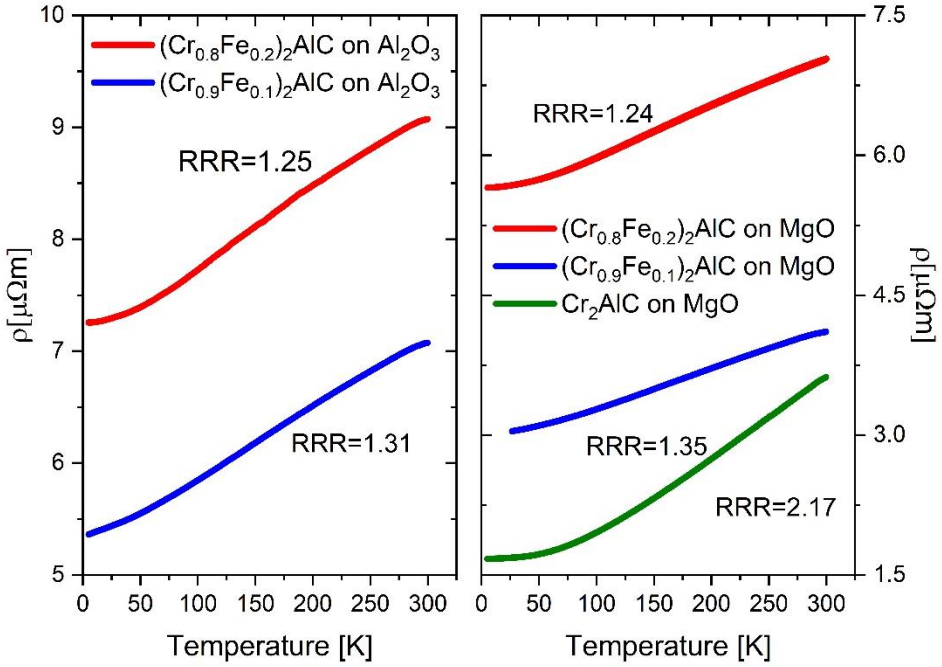

Figure 7. Temperature dependence of the resistivity for $(Cr_{0.9}Fe_{0.1})_2AlC$ and $(Cr_{0.8}Fe_{0.2})_2AlC$ thin films deposited on MgO(111) and Al_2O_3(0001) substrates. The resistivity dependence of parent Cr_2AlC thin film on MgO(111) substrate is presented as a reference.

The electrical resistivity values strongly depend on the Fe doping and less on the substrate choice. $(Cr_{0.8}Fe_{0.2})_2AlC$ on Al_2O_3(0001) exhibits an about $1.3_{T=2/300\ K}$ times higher resistivity than on MgO(111) for all temperatures, while the resistivity difference between the substrates for $(Cr_{0.9}Fe_{0.1})_2AlC$ changes by a factor of $1.8_{T=2\ K}$ and $1.7_{T=300\ K}$. With increasing Fe content, the resistivity rises by 30% for the samples on Al_2O_3(0001) and by 70%-90% for the films on MgO(111). The linear slope above about 100 K is smaller for $(Cr_{0.9}Fe_{0.1})_2AlC$ samples clearly

pointing together with the lower resistivity values towards less impurities in the films. This observation is supported by the pronounced lower resistivity and increased RRR of the parental Cr_2AlC on MgO(111). The synthesized films demonstrate overall low resistivity suggesting their potential as high conductive coatings [50, 51].

CONCLUSION

In this study we have shown that fine tuning of individual elemental deposition using PLD can be used to introduce Fe in the nanolaminated structure of the Cr_2AlC MAX phase. Following the density functional calculations predicting phase stability of $(Cr_{1-x}Fe_x)_2AlC$ for $x < 0.2$, we synthesized thin films with the target Fe content of $x = 0.1$ and $x = 0.2$ on MgO(111) and Al_2O_3(0001) using pure elemental targets at 600°C. For the $(Cr_{0.9}Fe_{0.1})_2AlC$ MAX phase we obtain the epitaxial relation $(Cr_{0.9}Fe_{0.1})_2AlC$ [11-20] || MgO [10-1]. Despite phase purity revealed by XRD and pole figure measurements for $x = 0.1$, the coexistence of the MAX phase structure and $(Cr,Fe)_5Al_8$ intermetallic compounds was resolved by HRTEM. Using PLD we incorporated up to $x = 0.068$ (3.4 at%) Fe in M-layers of the parental Cr_2AlC MAX phase which is the highest doping level obtained to date. Incorporation of Fe resulted in a slight reduction of the *c* lattice parameter having a similar but less pronounced effect on the *a* lattice parameter of Cr_2AlC MAX phase, resembling theoretical predictions. Despite the successful incorporation of Fe in the MAX phase structure, the presence of magnetic order has not been observed in our study. Electrical measurements revealed high metallic conductivity typical for MAX phases suggesting their potential as conductive coatings.

ASSOCIATED CONTENT

Supporting Information. The Supporting Information is available free of charge on the ACS Publications website. Additional information about the competing phases in $(Cr_{1-x}Fe_x)_2AlC$ MAX phase system, SEM images of the synthesized films with corresponding EDX elemental maps and vibrating sample magnetometry of $Al_2O_3(0001)$ substrate and $(Cr_{1-x}Fe_x)_2AlC$ MAX phase film.

AUTHOR INFORMATION

Corresponding Author

*Hanna Pazniak. E-mail: hanna.pazniak@uni-due.de,

*Ulf Wiedwald. E-Mail: ulf.wiedwald@uni-due.de

Author Contributions

The manuscript was written through contributions of all authors. All authors have given approval to the final version of the manuscript.

Funding Sources

This work has been supported by the Deutsche Forschungsgemeinschaft (DFG) within CRC/TRR 270, project B02 (Project-ID 405553726). The calculations were carried out using supercomputer resources provided by the Swedish National Infrastructure for Computing (SNIC) at the National Supercomputer Centre (NSC) and the High Performance Computing Center North (HPC2N) partially funded by the Swedish Research Council through grant agreement no. 2018-05973. J. R. acknowledges funding from the Knut and Alice Wallenberg Foundation. Support by the Interdisciplinary Center for Analytics on the Nanoscale (ICAN) of the University of Duisburg-Essen (DFG RIsources reference: RI_00313), a DFG-funded core facility (Project

Nos. 233512597 and 324659309), is gratefully acknowledged. M. F. acknowledges co-funding by the government of the Russian Federation (agreement No. 075-15-2019-1886).

Notes

The authors declare no competing financial interest.

ACKNOWLEDGMENT

We thank Merlin Schmuck and Doru Lupascu for assistance and providing access to the XRD with Eulerian cradle. Dr. Markus Heidelmann is acknowledged for the help in TEM. We also thank Soma Salamon and Ulrich von Hörsten for their support in the optimization of the deposition chamber.

REFERENCES

(1) Barsoum, M. W.; El-Raghy, T. The MAX Phases: Unique New Carbide and Nitride Materials: Ternary ceramics turn out to be surprisingly soft and machinable, yet also heat-tolerant, strong and lightweight. *American Scientist* **2001,** *89* (4), 334-343.

(2) Sokol, M.; Natu, V.; Kota, S.; Barsoum, M. W. On the Chemical Diversity of the MAX Phases. *Trends in Chemistry* **2019,** *1* (2), 210-223, DOI: 10.1016/j.trechm.2019.02.016.

(3) Radovic, M.; Barsoum, M. In *MAX phases : Bridging the gap between metals and ceramics MAX phases : Bridging the gap between metals and ceramics*, 2013.

(4) Lapauw, T.; Tytko, D.; Vanmeensel, K.; Huang, S.; Choi, P.-P.; Raabe, D.; Caspi, E. a. N.; Ozeri, O.; to Baben, M.; Schneider, J. M.; Lambrinou, K.; Vleugels, J. (Nbx, Zr1–x)4AlC3 MAX Phase Solid Solutions: Processing, Mechanical Properties, and Density Functional Theory

Calculations. *Inorganic Chemistry* **2016,** *55* (11), 5445-5452, DOI: 10.1021/acs.inorgchem.6b00484.

(5) Dubois, S.; Bei, G. P.; Tromas, C.; Gauthier-Brunet, V.; Gadaud, P. Synthesis, Microstructure, and Mechanical Properties of Ti3Sn(1−x)AlxC2 MAX Phase Solid Solutions. **2010,** *7* (6), 719-729, DOI: https://doi.org/10.1111/j.1744-7402.2010.02554.x.

(6) Hadi, M. A.; Panayiotatos, Y.; Chroneos, A. Structural and optical properties of the recently synthesized (Zr3−xTix)AlC2 MAX phases. *Journal of Materials Science: Materials in Electronics* **2017,** *28* (4), 3386-3393, DOI: 10.1007/s10854-016-5933-z.

(7) Meshkian, R.; Ingason, A. S.; Arnalds, U. B.; Magnus, F.; Lu, J.; Rosen, J. A magnetic atomic laminate from thin film synthesis: (Mo0.5Mn0.5)2GaC. **2015,** *3* (7), 076102, DOI: 10.1063/1.4926611.

(8) Siebert, J. P.; Mallett, S.; Juelsholt, M.; Pazniak, H.; Wiedwald, U.; Page, K.; Birkel, C. S. Structure determination and magnetic properties of the Mn-doped MAX phase Cr2GaC. *Materials Chemistry Frontiers* **2021**, DOI: 10.1039/D1QM00454A.

(9) Ingason, A. S.; Dahlqvist, M.; Rosen, J. Magnetic MAX phases from theory and experiments; a review. *Journal of Physics: Condensed Matter* **2016,** *28* (43), 433003, DOI: 10.1088/0953-8984/28/43/433003.

(10) Tao, Q.; Lu, J.; Dahlqvist, M.; Mockute, A.; Calder, S.; Petruhins, A.; Meshkian, R.; Rivin, O.; Potashnikov, D.; Caspi, E. a. N.; Shaked, H.; Hoser, A.; Opagiste, C.; Galera, R.-M.; Salikhov, R.; Wiedwald, U.; Ritter, C.; Wildes, A. R.; Johansson, B.; Hultman, L.; Farle, M.; Barsoum, M. W.; Rosen, J. Atomically Layered and Ordered Rare-Earth i-MAX Phases: A New Class of

Magnetic Quaternary Compounds. *Chemistry of Materials* **2019,** *31* (7), 2476-2485, DOI: 10.1021/acs.chemmater.8b05298.

(11) Petruhins, A.; Lu, J.; Hultman, L.; Rosen, J. Synthesis of atomically layered and chemically ordered rare-earth (RE) i-MAX phases; (Mo2/3RE1/3)2GaC with RE = Gd, Tb, Dy, Ho, Er, Tm, Yb, and Lu. *Materials Research Letters* **2019,** *7* (11), 446-452, DOI: 10.1080/21663831.2019.1644684.

(12) Anasori, B.; Dahlqvist, M.; Halim, J.; Moon, E. J.; Lu, J.; Hosler, B. C.; Caspi, E. a. N.; May, S. J.; Hultman, L.; Eklund, P.; Rosén, J.; Barsoum, M. W. Experimental and theoretical characterization of ordered MAX phases Mo2TiAlC2 and Mo2Ti2AlC3. **2015,** *118* (9), 094304, DOI: 10.1063/1.4929640.

(13) Ouisse, T.; Barsoum, M. W. Magnetotransport in the MAX phases and their 2D derivatives: MXenes. *Materials Research Letters* **2017,** *5* (6), 365-378, DOI: 10.1080/21663831.2017.1333537.

(14) Novoselova, I. P.; Petruhins, A.; Wiedwald, U.; Ingason, Á. S.; Hase, T.; Magnus, F.; Kapaklis, V.; Palisaitis, J.; Spasova, M.; Farle, M.; Rosen, J.; Salikhov, R. Large uniaxial magnetostriction with sign inversion at the first order phase transition in the nanolaminated Mn2GaC MAX phase. *Scientific Reports* **2018,** *8* (1), 2637, DOI: 10.1038/s41598-018-20903-2.

(15) Ingason, A. S.; Petruhins, A.; Dahlqvist, M.; Magnus, F.; Mockute, A.; Alling, B.; Hultman, L.; Abrikosov, I. A.; Persson, P. O. Å.; Rosen, J. A nanolaminated magnetic phase: Mn_2GaC. *Materials Research Letters* **2014,** *2* (2), 89-93, DOI: dx.doi.rg/10.1080/21663831.2013.865105.

(16) Dahlqvist, M.; Ingason, A. S.; Alling, B.; Magnus, F.; Thore, A.; Petruhins, A.; Mockute, A.; Arnalds, U. B.; Sahlberg, M.; Hjörvarsson, B.; Abrikosov, I. A.; Rosen, J. Magnetically driven anisotropic structural changes in the atomic laminate Mn2GaC. *Physical Review B* **2016,** *93* (1), 014410, DOI: 10.1103/PhysRevB.93.014410.

(17) Hamm, C. M.; Bocarsly, J. D.; Seward, G.; Kramm, U. I.; Birkel, C. S. Non-conventional synthesis and magnetic properties of MAX phases (Cr/Mn)2AlC and (Cr/Fe)2AlC. *Journal of Materials Chemistry C* **2017,** *5* (23), 5700-5708, DOI: 10.1039/C7TC00112F.

(18) Mockute, A.; Persson, P. O. Å.; Magnus, F.; Ingason, A. S.; Olafsson, S.; Hultman, L.; Rosen, J. Synthesis and characterization of arc deposited magnetic $(Cr,Mn)_2AlC$ MAX phase films. *physica status solidi (RRL) – Rapid Research Letters* **2014,** *8* (5), 420-423, DOI: 10.1002/pssr.201409087.

(19) Li, Y.; Lu, J.; Li, M.; Chang, K.; Zha, X.; Zhang, Y.; Chen, K.; Persson, P. O. Å.; Hultman, L.; Eklund, P.; Du, S.; Francisco, J. S.; Chai, Z.; Huang, Z.; Huang, Q. Multielemental single–atom-thick A layers in nanolaminated V2(Sn,A)C (A = Fe, Co, Ni, Mn) for tailoring magnetic properties. *PNAS* **2020,** *117* (2), 820-825, DOI: 10.1073/pnas.1916256117 .

(20) Lai, C.-C.; Petruhins, A.; Lu, J.; Farle, M.; Hultman, L.; Eklund, P.; Rosen, J. Thermally induced substitutional reaction of Fe into Mo2GaC thin films. *Materials Research Letters* **2017,** *5* (8), 533-539, DOI: 10.1080/21663831.2017.1343207.

(21) Maniv, A.; Reyes, A. P.; Ramakrishna, S. K.; Graf, D.; Huq, A.; Potashnikov, D.; Rivin, O.; Pesach, A.; Tao, Q.; Rosen, J.; Felner, I.; Caspi, E. N. Microscopic evidence for Mn-induced long range magnetic ordering in MAX phase compounds. *Journal of Physics: Condensed Matter* **2020,** *33* (2), 025803, DOI: 10.1088/1361-648x/abb998.

(22) Lin, S.; Huang, Y.; Zu, L.; Kan, X.; Lin, J.; Song, W.; Tong, P.; Zhu, X.; Sun, Y. Alloying effects on structural, magnetic, and electrical/thermal transport properties in MAX-phase Cr2−xMxGeC (M=Ti, V, Mn, Fe, and Mo). *Journal of Alloys and Compounds* **2016,** *680*, 452-461, DOI: https://doi.org/10.1016/j.jallcom.2016.04.197.

(23) Lin, S.; Tong, P.; Wang, B. S.; Huang, Y. N.; Lu, W. J.; Shao, D. F.; Zhao, B. C.; Song, W. H.; Sun, Y. P. Magnetic and electrical/thermal transport properties of Mn-doped Mn+1AXn phase compounds Cr2−xMnxGaC ($0 \leq x \leq 1$). *Journal of Applied Physics* **2013,** *113* (5), 053502, DOI: 10.1063/1.4789954.

(24) Hamm, C. M.; Dürrschnabel, M.; Molina-Luna, L.; Salikhov, R.; Spoddig, D.; Farle, M.; Wiedwald, U.; Birkel, C. S. Structural, magnetic and electrical transport properties of non-conventionally prepared MAX phases V2AlC and (V/Mn)2AlC. *Materials Chemistry Frontiers* **2018,** *2* (3), 483-490, DOI: 10.1039/c7qm00488e.

(25) Salikhov, R.; Semisalova, A. S.; Petruhins, A.; Ingason, A. S.; Rosen, J.; Wiedwald, U.; Farle, M. Magnetic Anisotropy in the (Cr0.5Mn0.5)2GaC MAX Phase. *Materials Research Letters* **2015,** *3* (3), 156-160, DOI: 10.1080/21663831.2015.1036324.

(26) Mockute, A.; Persson, P. O. Å.; Lu, J.; Ingason, A. S.; Magnus, F.; Olafsson, S.; Hultman, L.; Rosen, J. Structural and magnetic properties of (Cr1−xMnx)5Al8 solid solution and structural relation to hexagonal nanolaminates. *Journal of Materials Science* **2014,** *49* (20), 7099-7104, DOI: 10.1007/s10853-014-8416-8.

(27) Stevens, M.; Pazniak, H.; Jemiola, A.; Felek, M.; Farle, M.; Wiedwald, U. Pulsed laser deposition of epitaxial Cr2AlC MAX phase thin films on MgO(111) and Al2O3(0001). *Materials Research Letters* **2021,** *9* (8), 343-349, DOI: 10.1080/21663831.2021.1920510.

(28) Blöchl, P. E. Projector augmented-wave method. *Physical Review B* **1994,** *50* (24), 17953-17979, DOI: dx.doi.org/10.1103/PhysRevB.50.17953.

(29) Kresse, G.; Joubert, D. From ultrasoft pseudopotentials to the projector augmented-wave method. *Physical Review B* **1999,** *59* (3), 1758-1775, DOI: dx.doi.org/10.1103/PhysRevB.59.1758.

(30) Kresse, G.; Hafner, J. *Ab initio* molecular dynamics for liquid metals. *Physical Review B* **1993,** *47* (1), 558-561, DOI: dx.doi.org/10.1103/PhysRevB.47.558.

(31) Kresse, G.; Furthmüller, J. Efficiency of *ab-initio* total energy calculations for metals and semiconductors using a plane-wave basis set. *Computational Materials Science* **1996,** *6* (1), 15-50, DOI: dx.doi.org/10.1016/0927-0256(96)00008-0.

(32) Kresse, G.; Furthmüller, J. Efficient iterative schemes for *ab initio* total-energy calculations using a plane-wave basis set. *Physical Review B* **1996,** *54* (16), 11169-11186, DOI: dx.doi.org/10.1103/PhysRevB.54.11169.

(33) Perdew, J. P.; Burke, K.; Ernzerhof, M. Generalized gradient approximation made simple. *Physical Review Letters* **1996,** *77* (18), 3865-3868, DOI: dx.doi.org/10.1103/PhysRevLett.77.3865.

(34) Dahlqvist, M.; Alling, B.; Rosen, J. Correlation between magnetic state and bulk modulus of Cr_2AlC. *Journal of Applied Physics* **2013,** *113* (21), 216103.

(35) Dahlqvist, M.; Alling, B.; Rosen, J. A critical evaluation of GGA + *U* modeling for atomic, electronic and magnetic structure of Cr_2AlC, Cr_2GaC and Cr_2GeC. *Journal of Physics: Condensed Matter* **2015,** *27* (9), 095601.

(36) Monkhorst, H. J.; Pack, J. D. Special points for Brillouin-zone integrations. *Physical Review B* **1976,** *13* (12), 5188-5192, DOI: dx.doi.org/10.1103/PhysRevB.13.5188.

(37) Zunger, A.; Wei, S. H.; Ferreira, L. G.; Bernard, J. E. Special quasirandom structures. *Physical Review Letters* **1990,** *65* (3), 353-356, DOI: dx.doi.org/10.1103/PhysRevLett.65.353.

(38) Dahlqvist, M.; Alling, B.; Abrikosov, I. A.; Rosén, J. Phase stability of Ti_2AlC upon oxygen incorporation: A first-principles investigation. *Physical Review B* **2010,** *81* (2), 024111, DOI: dx.doi.org/10.1103/Physrevb.81.024111.

(39) Dahlqvist, M.; Alling, B.; Rosén, J. Stability trends of MAX phases from first principles. *Physical Review B* **2010,** *81* (22), 220102, DOI: dx.doi.org/10.1103/PhysRevB.81.220102.

(40) Eklund, P.; Dahlqvist, M.; Tengstrand, O.; Hultman, L.; Lu, J.; Nedfors, N.; Jansson, U.; Rosén, J. Discovery of the ternary nanolaminated compound Nb_2GeC by a systematic theoretical-experimental approach. *Physical Review Letters* **2012,** *109* (3), 035502, DOI: dx.doi.org/10.1103/PhysRevLett.109.035502.

(41) Ingason, A. S.; Mockute, A.; Dahlqvist, M.; Magnus, F.; Olafsson, S.; Arnalds, U. B.; Alling, B.; Abrikosov, I. A.; Hjörvarsson, B.; Persson, P. O. Å.; Rosen, J. Magnetic self-organized atomic laminate from first principles and thin film synthesis. *Physical Review Letters* **2013,** *110* (19), 195502, DOI: dx.doi.org/10.1103/PhysRevLett.110.195502.

(42) Mockute, A.; Dahlqvist, M.; Emmerlich, J.; Hultman, L.; Schneider, J. M.; Persson, P. O. Å.; Rosen, J. Synthesis and *ab initio* calculations of nanolaminated $(Cr,Mn)_2AlC$ compounds. *Physical Review B* **2013,** *87* (9), 094113, DOI: dx.doi.org/10.1103/PhysRevB.87.094113.

(43) Eason, R. *Pulsed Laser Deposition of Thin Films: Applications-Led Growth of Functional Materials*, Wiley: 2007.

(44) Dahlqvist, M.; Alling, B.; Abrikosov, I. A.; Rosen, J. Magnetic nanoscale laminates with tunable exchange coupling from first principles. *Physical Review B* **2011,** *84* (22), 220403, DOI: dx.doi.org/10.1103/PhysRevB.84.220403.

(45) Ohmer, D.; Qiang, G.; Opahle, I.; Singh, H. K.; Zhang, H. High-throughput design of 211-M2AX compounds. *Physical Review Materials* **2019,** *3* (5), 053803, DOI: 10.1103/PhysRevMaterials.3.053803.

(46) Manoun, B.; Kulkarni, S.; Pathak, N.; Saxena, S. K.; Amini, S.; Barsoum, M. W. Bulk moduli of Cr_2GaC and Ti_2GaN up to 50 GPa. *Journal of Alloys and Compounds* **2010,** *505* (1), 328-331, DOI: http://dx.doi.org/10.1016/j.jallcom.2010.06.066.

(47) Cabioch, T.; Eklund, P.; Mauchamp, V.; Jaouen, M.; Barsoum, M. W. Tailoring of the thermal expansion of $Cr_2(Al_x,Ge_{1-x})C$ phases. *Journal of the European Ceramic Society* **2013,** *33* (4), 897-904, DOI: 10.1016/j.jeurceramsoc.2012.10.008.

(48) Petruhins, A.; Ingason, A. S.; Lu, J.; Magnus, F.; Olafsson, S.; Rosen, J. Synthesis and characterization of magnetic (Cr0.5Mn0.5)2GaC thin films. *Journal of Materials Science* **2015,** *50* (13), 4495-4502, DOI: 10.1007/s10853-015-8999-8.

(49) Trautvetter, M.; Wiedwald, U.; Paul, H.; Minkow, A.; Ziemann, P. Thermally driven solid-phase epitaxy of laser-ablated amorphous AlFe films on (0001)-oriented sapphire single crystals. *Applied Physics A* **2011,** *102* (3), 725-730, DOI: 10.1007/s00339-010-5972-x.

(50) Wang, Z.; Ma, G.; Li, Z.; Ruan, H.; Yuan, J.; Wang, L.; Ke, P.; Wang, A. Corrosion mechanism of Ti_2AlC MAX phase coatings under the synergistic effects of water vapor and solid NaCl at 600 ^oC. Corrosion Science **2021** *192*, 109788, DOI: 10.1016/j.corsci.2021.109788.

(51) Ma, G.; Zhang, D.; Guo, P.; Li, H.; Xin, Y.; Wang, Z.; Wang, A. Phase orientation improved the corrosion resistance and conductivity of Cr_2AlC coatings for metal bipolar plates. *Journal of Materials Science & Technology* **2022**, *105*, 36-44, DOI: 10.1016/j.jmst.2021.06.069.

Table of Content